Quantum superpositions and entanglement of thermal states at high temperatures and their applications to quantum-information processing

Hyunseok Jeong and Timothy C. Ralph

Centre for Quantum Computer Technology, Department of Physics, University of Queensland, St. Lucia, Qld 4072, Australia

We study characteristics of superpositions and entanglement of thermal states at high temperatures and discuss their applications to quantum-information processing. We introduce thermal-state qubits and thermal-Bell states, which are a generalization of pure-state qubits and Bell states to thermal mixtures. A scheme is then presented to discriminate between the four thermal-Bell states without photon number resolving detection but with Kerr nonlinear interactions and two single-photon detectors. This enables one to perform quantum teleportation and gate operations for quantum computation with thermal-state qubits.

I. INTRODUCTION

In many problems considered within the framework of quantum physics, physical systems are treated as pure states that can be represented by state vectors, or equivalently, by wave functions. Even though such an approach is simple and useful to address certain problems, it could often be quite different from real conditions of physical systems. This may be particularly true when one deals with macroscopic physical systems in terms of quantum physics. A macroscopic object is a complex open system, which cannot avoid continuous interactions with the environment. Such a physical system is generally in a significantly mixed state and cannot be represented by a state vector. In general, mixed states are subtle objects whose properties are significantly more difficult to characterize than pure states.

Schrödinger's famous cat paradox [1] is a typical example where a massive classical object was assumed to be a pure state. It describes a counterintuitive feature of quantum physics, which dramatically appears when the principle of quantum superposition is applied to macroscopic objects. In the original paradox and its various explanations, the initial cat isolated in the steel chamber is considered a pure state that can be represented by a state vector such as $|\text{alive}\rangle$ (or a wave function such as ψ_{alive}). The cat isolated from the environment is then assumed to interact with a microscopic superposition state $(|g\rangle+|e\rangle)/\sqrt{2}$, where $|g\rangle$ and $|e\rangle$ are the ground and excited states of a two-level atom. The cat will be dead if the atom is found in the excited state $|e\rangle$, while it will remain alive if otherwise. Thus in Schrödinger's gedanken experiment the cat is entangled with the atom as $(|g\rangle|\text{alive}\rangle+|e\rangle|\text{dead}\rangle)\sqrt{2}$, where the alive and dead statuses of the cat are described by the state vectors $|\text{alive}\rangle$ and $|\text{dead}\rangle$. If one measures out the atomic system on the superposed basis $(|g\rangle\pm|e\rangle)/\sqrt{2}$, the cat will be in a superposition of alive and dead states such as $(|\text{alive}\rangle\pm|\text{dead}\rangle)/\sqrt{2}$. It is often argued that such superposed states and entangled states can theoretically exist but are virtually impossible to observe because one cannot perfectly isolate a macroscopic object such as the cat from its environment [2].

However, this explanation is not fully satisfactory because the cat, a macroscopic object, is a complex open system, which cannot be represented by a state vector. One may ar-

gue that the cat could be assumed to be in an *unknown* pure state such that the cat was certainly alive but the exact state of the cat was unknown. However, the interactions between the cat and its environment can cause the cat to become entangled with the environment [3]. In such a case, even though one can perfectly isolate the cat in the steel chamber from the environment, the cat will remain entangled with the environment due to its preinteractions with the environment. Therefore, strictly speaking, even to assume a cat as an unknown pure state in the steel chamber is not legitimate. Thus a key point here is that it is unsatisfactory to describe the cat by a pure state such as $|\text{alive}\rangle$ and $|\text{dead}\rangle$. We may need a more realistic assumption that the "cat" in Schrödinger's paradox was in a significantly mixed classical state. An intriguing question is then whether the quantum properties of the resulting state would still remain or diminish under such an assumption.

Recently, such an analogy of Schrödinger's cat paradox, where the state corresponding to the virtual cat is a significantly mixed thermal state, was investigated [4]. A thermal state with a high temperature is considered a classical state in quantum optics. As the temperature of the thermal state increases, the degree of mixedness, which can be quantified by linear entropy, rapidly approaches the maximum value. When the temperature approaches infinity, the thermal state does not show any quantum properties. As a comparison, coherent states with large amplitudes are known as the most classical pure states [5], and their superposition is often regarded as a superposition of classical states [6]. However, coherent states are still pure states, which may not well represent truly classical systems, and they display some nonclassical features [7]. In Ref. [4], it was shown that prominent quantum properties can actually be transferred from a microscopic superposition to a significantly mixed thermal state (i.e., a thermal state of which the degree of mixedness is close to the maximum value) at a high temperature through an experimentally feasible process. This result clarifies that unavoidable initial mixedness of the cat does not preclude strong quantum phenomena.

One of the results in Ref. [4] is that quantum entanglement can be produced between thermal states with nearly the maximum Bell-inequality violation when the temperatures of both modes goes to infinity. In previous related results, Bose

et al. showed that entanglement can arise when two systems interact if one of the systems is pure even when the other system is extremely mixed [8]. There is an interesting previous example shown by Filip *et al.* for the maximum violation of Bell's inequality when one of the modes is an extremely mixed thermal state [9]. Very recently, Ferreira *et al.* showed that entanglement can be generated at any finite temperature between high-Q cavity mode field and a movable mirror thermal state [10]. However, in these examples [8–10] only one of the modes is considered a large thermal state [8–10] and entanglement vanishes in the infinite temperature limit [8,10], which is obviously in contrast to the result presented in Ref. [4]. Entanglement for both of the modes at the thermal limit of the infinitely high temperature has not been found before. Remarkably, the violation of Bell's inequality in our examples reaches up to Cirel'son's bound [11] even in this infinite-temperature limit for both modes. As Vedral [12] and Ferreira *et al.* [10] pointed out it is believed that high temperatures reduce entanglement and all entanglement vanishes if the temperature is high enough, which is obviously not the case in Ref. [4].

The purpose of this paper is twofold. First, we review and further investigate various properties of superpositions and entanglement of thermal states at high temperatures [4]. In particular, we investigate two classes of highly mixed symmetric states in the phase space. Both the classes of these states do not show typical interference patterns in the phase space while they manifest strong singular behaviors. Interestingly, the first class of states has neither squeezing properties nor negative values in their Wigner functions, however, they are found to be highly nonclassical states. The second class of states has the maximum negativity in the Wigner function. Further, we discuss the possibility of quantum information processing with thermal-state qubits. We introduce thermal-state qubits and thermal-Bell states, which are a generalization of pure Bell states. We show that four thermal-Bell states can be well discriminated by nonlinear interactions without photon number resolving measurements. Quantum teleportation and gate operations for thermal-state qubits can be realized using the Bell measurement scheme.

This paper is organized as follows. In Sec. II, we review the generation process of superpositions of thermal states and study their characteristics. In Sec. III, we study entanglement of thermal states, i.e., Bell inequality violations. In Sec. IV, we discuss the possibility of quantum-information processing using thermal states. We first define the thermal-state qubit and the Bell-basis states using thermal-state entanglement. We then show that the four Bell states can be well discriminated by homodyne detection and two Kerr nonlinearities. It follows that quantum teleportation and quantum gate operations can be realized with thermal-state qubits. We conclude with final remarks in Sec. V.

II. SUPERPOSITIONS OF THERMAL STATES

A. Generation of thermal-state superpositions

Let us first consider a two-mode harmonic oscillator system. A displaced thermal state can be defined as

$$\rho^{\text{th}}(V,d) = \int d^2\alpha P^{\text{th}}(V,d)|\alpha\rangle\langle\alpha|, \tag{1}$$

where $|\alpha\rangle$ is a coherent state of amplitude α and

$$P_\alpha^{\text{th}}(V,d) = \frac{2}{\pi(V-1)} \exp\left[-\frac{2|\alpha-d|^2}{V-1}\right], \tag{2}$$

with variance V and displacement d in the phase space. The thermal temperature τ increases as V increases as $e^{\hbar\nu/\tau} = (V+1)/(V-1)$, where $\hbar$ is Planck's constant and ν is the frequency [13]. Suppose that a microscopic superposition state

$$|\psi\rangle_a = \frac{1}{\sqrt{2}}(|0\rangle_a + |1\rangle_a), \tag{3}$$

where $|0\rangle$ and $|1\rangle$ are the ground and first excited states of the harmonic oscillator, interacts with a thermal state $\rho_b^{\text{th}}(V,d)$ and the interaction Hamiltonian is

$$\mathcal{H}_K = \lambda\hat{a}^\dagger\hat{a}\hat{b}^\dagger\hat{b}, \tag{4}$$

which corresponds to the cross Kerr nonlinear interaction. The resulting state is then

$$\rho_{ab}^{\text{ent}} = \frac{1}{2}\int d^2\alpha P^{\text{th}}(V,d)\{|0\rangle\langle0|\otimes|\alpha\rangle\langle\alpha| + |1\rangle\langle0|\otimes|\alpha e^{i\varphi}\rangle\langle\alpha|$$
$$+ |0\rangle\langle1|\otimes|\alpha\rangle\langle\alpha e^{i\varphi}| + |1\rangle\langle1|\otimes|\alpha e^{i\varphi}\rangle\langle\alpha e^{i\varphi}|\}, \tag{5}$$

and φ is determined by the strength of the nonlinearity λ and the interaction time. The Wigner representation of ρ_{ab}^{ent} is

$$W_{ab}^{\text{ent}}(\alpha,\beta) = \frac{1}{\pi}e^{-2|\alpha|^2}\{W^{\text{th}}(\beta;d) + 2\alpha V^c(\beta;d) + 2[\alpha V^c(\beta;d)]^*$$
$$+ (4|\alpha|^2-1)W^{\text{th}}(\beta;de^{i\varphi})\}, \tag{6}$$

where α and β are complex numbers parametrizing the phase spaces of the microscopic and macroscopic systems, respectively, and

$$W^{\text{th}}(\alpha;d) = \frac{2}{\pi V} \exp\left[-\frac{2|\alpha-d|^2}{V}\right], \tag{7}$$

$$V^c(\alpha;d) = \frac{2}{\pi JK} \exp\left[-\frac{2}{K}(1-e^{i\varphi})d^2\right.$$
$$\left. -\frac{1}{J}\left(\alpha-\frac{2e^{i\varphi}d}{K}\right)\left(\alpha^*-\frac{2d}{K}\right)\right], \tag{8}$$

$K = 2 + (V-1)(1-e^{i\varphi})$, $J = (\sin\varphi/2 + iV\cos\varphi/2)/(2V\sin\varphi/2 + 2i\cos\varphi/2)$, and d has been assumed real without loss of generality. If one traces ρ_{ab}^{ent} over mode a, the remaining state will be simply in a classical mixture of two thermal states and its Wigner function will be positive everywhere. However, if one measures out the "microscopic part" on the superposed basis, i.e., $(|0\rangle_a \pm |1\rangle_a)/\sqrt{2}$, the "macroscopic part" for mode b may not lose its nonclassical characteristics. Such a measurement on the superposed basis will reduce the remaining state to

$$\rho^{\text{sup}(\pm)} = \mathcal{N}_s^{\pm} \int d^2\alpha P^{\text{th}}(V,d)\{|\alpha\rangle\langle\alpha| \pm |\alpha e^{i\varphi}\rangle\langle\alpha| \pm |\alpha\rangle\langle\alpha e^{i\varphi}|$$
$$+ |\alpha e^{i\varphi}\rangle\langle\alpha e^{i\varphi}|\}, \quad (9)$$

where $\mathcal{N}_s^{\pm}$ are the normalization factors, and its Wigner function is

$$W^{\text{sup}(\pm)}(\alpha) = \mathcal{N}_s^{\pm}\{W^{\text{th}}(\alpha;d) \pm V^c(\alpha;d) \pm \{V^c(\alpha;d)\}^*$$
$$+ W^{\text{th}}(\alpha;de^{i\varphi})\}. \quad (10)$$

The $\pm$ signs in Eqs. (8) and (9) correspond to the two possible results from the measurement of the microscopic system. The state in Eq. (10) is a superposition of two thermal states.

A feasible experimental setup to generate superpositions of thermal states is atom-field interactions in cavities, where a $\pi/2$ pulse can be used to prepare the atom in a superposed state. This type of experiment has already been performed to produce a superposition of coherent states [14]. In our cases, simply thermal states can be used instead of coherent states. Another possible setup is an all-optical scheme with free-traveling fields and a cross-Kerr medium, where a standard single-photon qubit could be used as the microscopic superposition. Recently, there have been theoretical and experimental efforts to produce and observe giant Kerr nonlinearities using electromagnetically induced transparency [15]. Furthermore, it was shown that a weak Kerr nonlinearity can still be useful if an initially strong field is employed in this type of experiment [16]. We shall further explain this with examples in Sec. III.

B. Negativity of the Wigner function

The negativity of the Wigner function is known as an indicator of nonclassicality of quantum states. In order to observe negativity of the Wigner function in a real experiment, its absolute minimum negativity should be large enough. The minimum negativity of the Wigner function in Eq. (6) for $V=1$ is -0.144 for $d=0$ and -0.246 for $d\to\infty$. Now suppose the initial state can be considered a classical thermal state by letting $V\gg 1$. One might expect that the negativity would be washed out as the initial state becomes mixed, but this is not the case. The minimum negativity actually increases as V gets larger. If $V\to\infty$, the minimum negativity of the Wigner function (6) is -0.246 regardless of d: no matter how mixed the initial thermal state was, the minimum negativity of the Wigner function is found to be a large value. The point in the phase space, which gives the minimum negativity when $V\gg 1$ or $d\gg 0$, is $(-\frac{1}{2},0)$ and has negativity

$$W_{\text{neg}} \equiv W_{ab}^{\text{ent}}\left(-\frac{1}{2},0\right) = \frac{2\left(-2 + \frac{1}{V}\exp\left[-\frac{2d^2}{V}\right]\right)}{\pi^2\sqrt{e}}. \quad (11)$$

It can be shown that W_{neg} approaches $-4/(\pi^2\sqrt{e}) \approx -0.246$ when either $d\to\infty$ or $V\to\infty$.

This effect is obviously due to the interaction between the microscopic superposition and the macroscopic thermal state. If the initial microscopic state is not superposed, e.g., $|\psi\rangle_a = |1\rangle_a$, the resulting state will be a simple direct product $(|1\rangle\langle 1|)_a \otimes \rho_b^{\text{th}}(V,-d)$. While for $V=1$ this state will exhibit negativity, this is washed out and tends to zero as $V\to\infty$. Needless to say, if it was $|0\rangle_a$ instead of $|1\rangle_a$, the resulting Wigner function will be a direct product of two Gaussian states whose Wigner function can never be negative. The superposition state (3) plays the crucial role in making the minimum negativity of the resulting Wigner function always saturate to a certain negative value no matter how mixed and classical the initial state of the other mode becomes.

The Wigner functions of the single-mode states $W^{\text{sup}(\pm)} \times(\alpha)$ in Eq. (10) show large negative values. The minimum negativity of the Wigner function $W^{\text{sup}(-)}(\alpha)$ is $W^{\text{sup}(-)}(0) = 2/\pi$ regardless of the values of V and d. On the other hand, the minimum negativity of the Wigner function $W^{\text{sup}(+)}(\alpha)$ approaches $2/\pi$ for $d\to\infty$ and disappears when $d=0$.

C. Quantum interference in the phase space

When $\varphi=\pi$, the state (9) becomes

$$\rho^{\pm} = N[\rho^{\text{th}}(V,d) \pm \sigma(V,d) \pm \sigma(V,-d) + \rho^{\text{th}}(V,-d)], \quad (12)$$

where $\sigma(V,d)=\int d^2\alpha P^{\text{th}}(V,d)|-\alpha\rangle\langle\alpha|$ and

$$N = 2\left(1 \pm \frac{\exp\left[-\frac{2d^2}{V}\right]}{V^2}\right). \quad (13)$$

If the initial state for mode b is a pure coherent state, i.e., $V=1$, the measurement on the superposed basis for mode a will produce a superposition of two pure coherent states as

$$|\widetilde{\Psi}_{\pm}\rangle = \frac{1}{\sqrt{1 \pm e^{-2|\alpha|^2}}}(|\alpha\rangle \pm |-\alpha\rangle), \quad (14)$$

where $\alpha=d$. The probability $\mathcal{P}_{\pm}$ to obtain the state $\rho^{\pm}$ is obtained as [17]

$$\mathcal{P}_{\pm} = \langle\psi^{\pm}|\text{Tr}_b[\rho_{ab}^{\text{ent}}]|\psi^{\pm}\rangle = \frac{1}{2}\left(1 \pm \frac{\exp\left[-\frac{2d^2}{V}\right]}{V}\right), \quad (15)$$

where $|\psi^{\pm}\rangle=(|0\rangle\pm|1\rangle)/\sqrt{2}$. The probability approaches $\mathcal{P}_{\pm}=1/2$ when either d or V becomes large.

As an analogy of Schrödinger's cat paradox, the variance V corresponds to the size of the initial "cat," and the distance d between the two thermal component states corresponds to distinguishability between the "alive cat" and the "dead cat". Suppose that both V and d are very large for the initial thermal state. The two thermal states $\rho^{th}(V,\pm d)$ become macroscopically distinguishable when $d\gg\sqrt{V}$, and our example may become a more realistic analogy of the cat paradox in this limit. Both the states $\rho^{\pm}$ in this case show probability distributions with two Gaussian peaks and interference fringes [4]. Figure 1 presents the probability distributions of x ($\equiv\text{Re}[\alpha]$) and p ($\equiv\text{Im}[\alpha]$) for ρ^- (a) when $V=100$ and $d=100$ and (b) when $V=1000$ and $d=300$. The probability
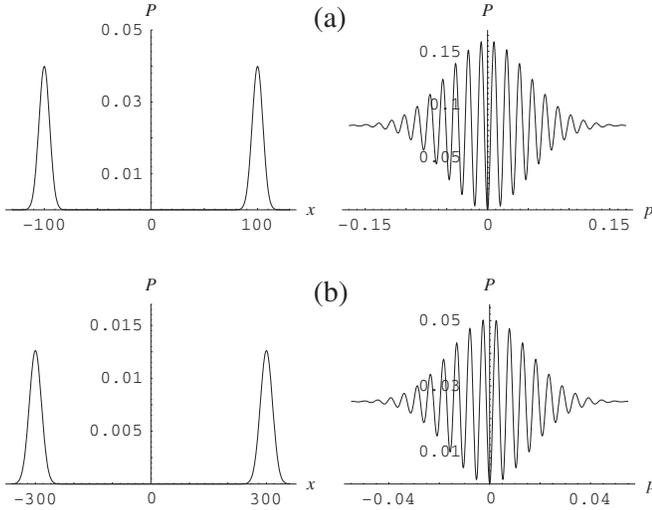
FIG. 1. The probability distributions of x (left) and p (right) for a "superposition" of two distant thermal states. A thermal state with a large mixedness is converted to such a "thermal-state superposition" by interacting with a microscopic superposition (see text). The variance V and displacement d for the thermal state are chosen as (a) $V=100$ and $d=100$, and (b) $V=1000$ and $d=300$. The fringe visibility is 1 regardless of V and the fringe spacing (the distance between the fringes) does not depend on the variance (i.e., mixedness) but only on the distance d between the two component thermal states.

distribution of x (p) for $\rho^{\pm}$ can be obtained by integrating the Wigner function of $\rho^{\pm}$ over p (x). The two Gaussian peaks along the x axis and interference fringes along the p axis shown in Fig. 1 are a typical signature of a quantum superposition between macroscopically distinguishable states. The visibility v of the interference fringes is defined as [13]

$$v = \frac{I_{\max} - I_{\min}}{I_{\max} + I_{\min}}, \qquad (16)$$

where $I = \int dx\, W^{\mathrm{sup}(-)}(\alpha)$ and the maximum should be taken over p. It can be simply shown that the visibility v is always 1 regardless of the value of V. Note that d should increase proportionally to $\sqrt{V}$ to maintain the condition of classical distinguishability between the two component thermal states $\rho^{\mathrm{th}}(V, \pm d)$. The interference fringes with high visibility are incompatible with classical physics and evidence of quantum coherence. The fringe spacing (the distance between the fringes) does not depend on V but only on d, i.e., a pure superposition of coherent states shows the same fringe spacing for a given d. We emphasize that the states shown in Fig. 1 are "superpositions" of severely mixed thermal states.

An experimental realization of a nonlinear effect corresponding to $\varphi = \pi$ is very demanding particularly in the presence of decoherence. Here we point out that the method using a weak nonlinear effect ($\varphi \ll \pi$) combined with a strong field ($d \gg 1$) [16] can be useful to generate a thermal-state superposition with prominent interference patterns. In Fig. 2, we have used experimentally accessible values $V=5$, $d=2000$, and $\varphi = \pi/1000$, but the fringe visibility is still 1. In
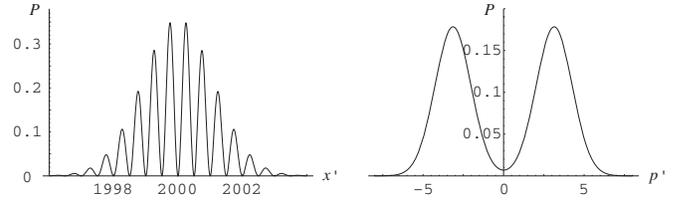
FIG. 2. The probability distributions P for a "superposition" of thermal states where $V=5$, $d=2000$, $\varphi = \pi/1000$. The x' (p') axis in this figure has been rotated by $\pi/2000$ from the x (p) axis for clarity.

this case, *decoherence during the nonlinear interaction would be significantly reduced* because of the decrease of the interaction time [16]. Note also that, if required, the state in Fig. 2 can be moved to the center of the phase space, for example, using a biased beam splitter (BS) and a strong coherent field [16].

D. Symmetric macroscopic quantum states

Let us assume that $d=0$, i.e., the initial state is the thermal state $\rho^{\mathrm{th}}(V,0)$ at the origin of the phase space. In this case, the thermal-state superpositions $\rho^{\pm}$ are produced with probabilities $\mathcal{P}_{\pm} = (1/2)\{1 \pm (1/V)\}$, respectively. Figure 3 shows the Wigner functions of ρ^{+} dependent on the interaction time between the macroscopic thermal state and the microscopic superposition in a cross-Kerr medium. The state is always symmetric in the phase space regardless of the interaction time as shown in Fig. 3. In this figure, the initial state is a thermal state of $V=100$ [Fig. 3(a)]. In a relatively short time ($\theta = \pi/32$ and $\theta = \pi/16$), the state shows some interference patterns. When $\theta = \pi$, the evolved state looks very localized around the origin as shown in Fig. 3. The generated state at $\theta = \pi$ does not show negativity of the Wigner function nor squeezing properties. On the other hand, a well defined P function does not exist for this state.

In the case of ρ^{-}, with the same assumption $d=0$, the Wigner function at $\varphi = \pi$ has the minimum negativity $(-2/\pi)$ at the origin regardless of V. As a result of the interaction with the microscopic superposition, a deep hole to the negative direction below zero has been formed around the origin for ρ^{-} as shown in Fig. 4.

III. ENTANGLEMENT BETWEEN THERMAL STATES

Entanglement between macroscopic objects and its Bell-type inequality tests are an important issue. In this section, we shall show that entanglement can be generated between high-temperature thermal states even when the temperature of each mode goes to infinity.

A. Entanglement using two initial thermal states

If the microscopic superposition interacts with two thermal states $\rho_b^{\mathrm{th}}(V,d)$ and $\rho_c^{\mathrm{th}}(V,d)$, and the microscopic particle is measured out on the superposed basis, the resulting state will be
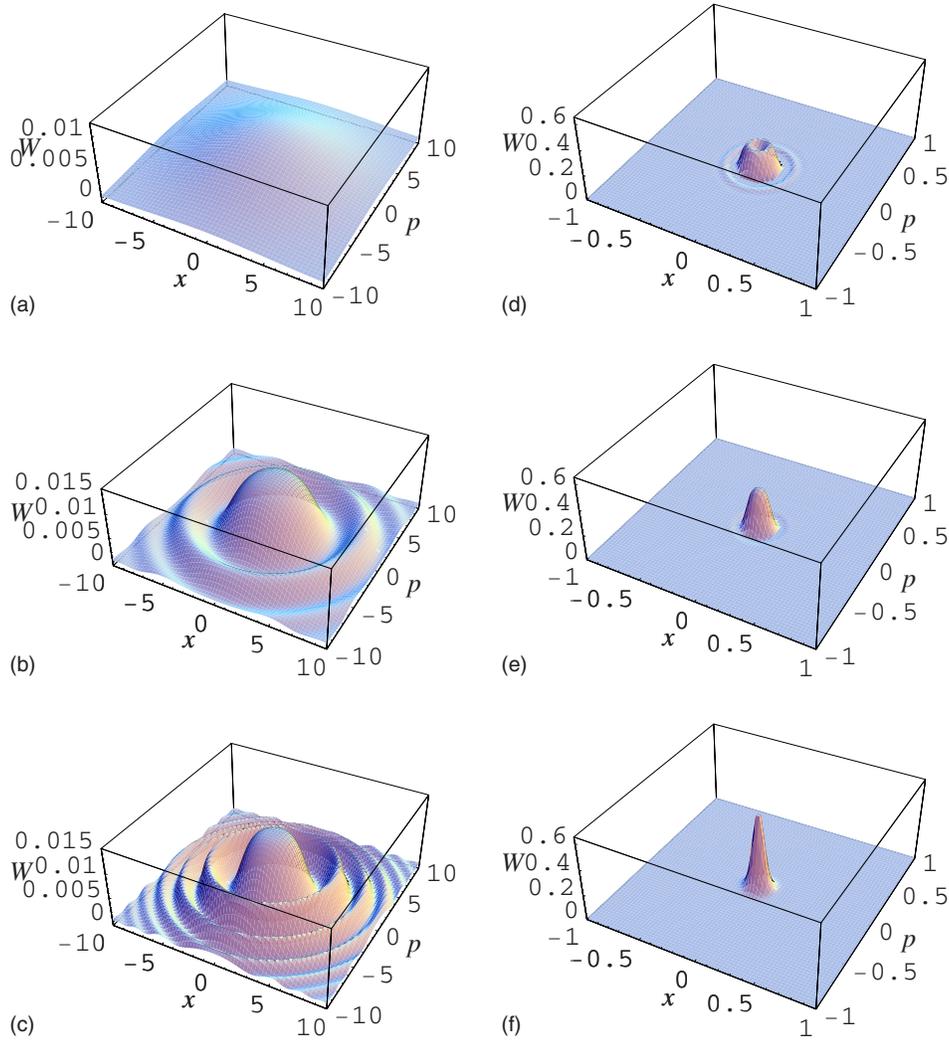
FIG. 3. (Color online) The time dependent Wigner functions of the thermal state of $V=100$ at the origin $(d=0)$ after an interaction with a microscopic superposition and a conditional measurement. The measurement result on the microscopic part was supposed to be $(|0\rangle + |1\rangle)/\sqrt{2}$. The interaction times are (a) $\theta=\lambda t=0$, (b) $\theta=\lambda t=\pi/32$, (c) $\theta=\pi/16$, (d) $\theta\approx 3.102$, (e) $\theta\approx 3.122$, and (f) $\theta=\pi$.

$$\rho^{tm(\pm)} = N_t\{\rho^{th}(V,d) \otimes \rho^{th}(V,d) \pm \sigma(V,d) \otimes \sigma(V,d)$$
$$\pm \sigma(V,-d) \otimes \sigma(V,-d) + \rho^{th}(V,-d) \otimes \rho^{th}(V,-d)\},$$
$$(17)$$

where

$$N_t = 2\left(1 \pm \frac{\exp\left[-\dfrac{4d^2}{V}\right]}{V^2}\right). \qquad (18)$$

Such two-mode thermal-state entanglement can be generated using two cavities and an atomic state detector [18]. Extending the two cavities to N cavities, entanglement of N-mode thermal states can also be generated. Such a state is an analogy of the N-mode pure GHZ state [19] but each mode is extremely mixed. Here we shall consider the Bell-CHSH inequality [20,21] with photon number parity measurements [18,22]. The parity measurements can be performed in a high-Q cavity using a far-off-resonant interaction between a two-level atom and the field [23]. The Bell-CHSH inequality can be represented in terms of the Wigner function as [22]

$$|B^{(\pm)}| = \frac{\pi^2}{4}|W^{tm(\pm)}(\alpha,\beta) + W^{tm(\pm)}(\alpha,\beta') + W^{tm(\pm)}(\alpha',\beta)$$
$$- W^{tm(\pm)}(\alpha',\beta')| \le 2, \qquad (19)$$

where $W^{tm(\pm)}(\alpha,\beta)$ is the Wigner function of $\rho^{tm(\pm)}$ in Eq. (17). As shown in Fig. 5, the Bell violation approaches the maximum bound for a bipartite measurement $2\sqrt{2}$ [11] when $d \gg \sqrt{V}$ regardless of the level of the mixedness V, i.e., the temperatures of the thermal states. Note that it is true for both of ρ_+ and ρ_- even though only the case of ρ_+ has been plotted in Fig. 5(a). This implies that entanglement of nearly 1 ebit has been produced between the two significantly mixed thermal states for $d \gg \sqrt{V}$, and such "thermal-state entanglement" cannot be described by a local theory.
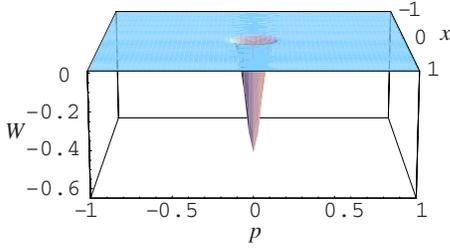
FIG. 4. (Color online) The Wigner function of the thermal state of $V=100$ at the origin ($d=0$) after an interaction with a microscopic superposition and a conditional measurement. The measurement result on the microscopic part was supposed to be $(|0\rangle - |1\rangle)/\sqrt{2}$ with the interaction time $\theta = \lambda t = \pi$.

B. Entanglement using a beam splitter

A different type of macroscopic entanglement can be generated by applying the beam splitter operation

$$\exp[\theta/2(e^{i\phi}\hat{a}_s^\dagger\hat{a}_d - e^{-i\phi}\hat{a}_d^\dagger\hat{a}_s)], \tag{20}$$

on the "thermal-state superpositions" in Eq. (9). The state after passing through a 50:50 beam splitter can be represented as

(a)

(b)
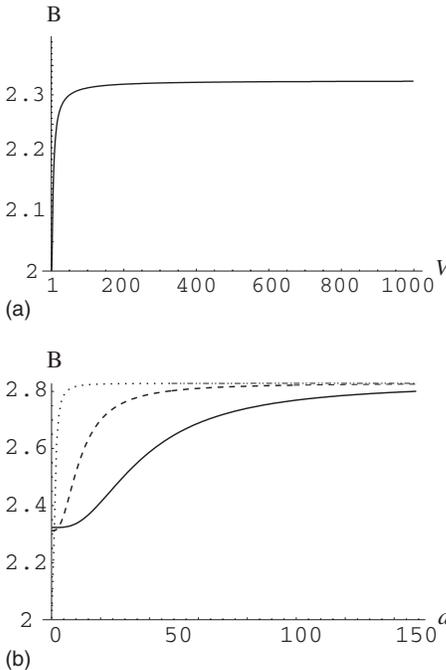
FIG. 5. (a) The optimized violation $B \equiv |B^+|_{\text{max}}$ of Bell-CHSH inequality for the "thermal-state entanglement" ρ_+ of $V=1000$ (solid curve) and $V=100$ (dashed curve). The Bell violation of a pure entangled coherent state, i.e., $V=1$, has been plotted for comparison (dotted curve). The Bell-violation B approaches its maximum bound $2\sqrt{2}$, when $d \gg \sqrt{V}$ regardless of the level of the mixedness V. (b) The optimized Bell-violation B against d for the different type of thermal-state entanglement generated using a 50:50 beam splitter from ρ^+. $V=1000$ (solid curve), $V=100$ (dashed curve), and $V=1$ (dotted curve).
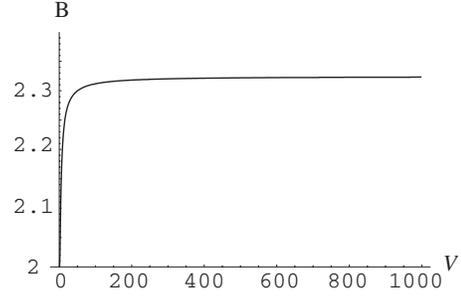
FIG. 6. The optimized Bell-violation B against V for the slightly different type of thermal-state entanglement generated using a 50:50 beam splitter using ρ^+ when $d=0$.

$$N\int d^2\alpha P_\alpha^{\text{th}}(V,d)\left(\left|\frac{\alpha}{\sqrt{2}},-\frac{\alpha}{\sqrt{2}}\right\rangle \pm \left|-\frac{\alpha}{\sqrt{2}},\frac{\alpha}{\sqrt{2}}\right\rangle\right)$$
$$\times\left(\left\langle\frac{\alpha}{\sqrt{2}},-\frac{\alpha}{\sqrt{2}}\right| \pm \left\langle-\frac{\alpha}{\sqrt{2}},\frac{\alpha}{\sqrt{2}}\right|\right), \tag{21}$$

where N is defined in Eq. (13). When d is large, this state violates the Bell-CHSH inequality to the maximum bound $2\sqrt{2}$ regardless of the level of mixedness V as shown in Fig. 5(b). Again, it is true for both ρ_+ and ρ_- even though only the case of ρ_+ has been plotted in Fig. 5(b). Furthermore, these states severely violate Bell's inequality even when $d=0$ as V increases as shown in Fig. 6. We have found that the optimized Bell violation of these states approaches 2.324 49 for $V \to \infty$. Interestingly, this value is exactly the same as the optimized Bell-CHSH violation for a pure two-mode squeezed state in the infinite squeezing limit [24]. Note that multimode entangled states can be generated using multiple beam splitters.

It should be noted that the Bell violations are more sensitive to the interaction time when either V or d is larger. Figure 7 clearly shows this tendency. Therefore, in order to observe the Bell violations using the mixed state of V (and d) large, the interaction time in the Kerr medium should be more accurate.

IV. QUANTUM-INFORMATION PROCESSING WITH THERMAL-STATE QUBITS

In this section, we discuss the possibility of quantum-information processing with thermal-state qubits and thermal-state entanglement.

A. Qubits and Bell-state measurements

We introduce a thermal-state qubit

$$\rho^\psi = |a|^2\rho^{\text{th}}(V,d) \pm ab^*\sigma(V,d) \pm a^*b\sigma(V,-d) + |b|^2\rho^{\text{th}}(V,-d), \tag{22}$$

where a and b are arbitrary complex numbers. The basis states $\rho^{\text{th}}(V,d)$ and $\rho^{\text{th}}(V,-d)$ can be well discriminated by a homodyne measurement when d is larger than V. The thermal-state qubit (22) can be rewritten as

(a)

(b)
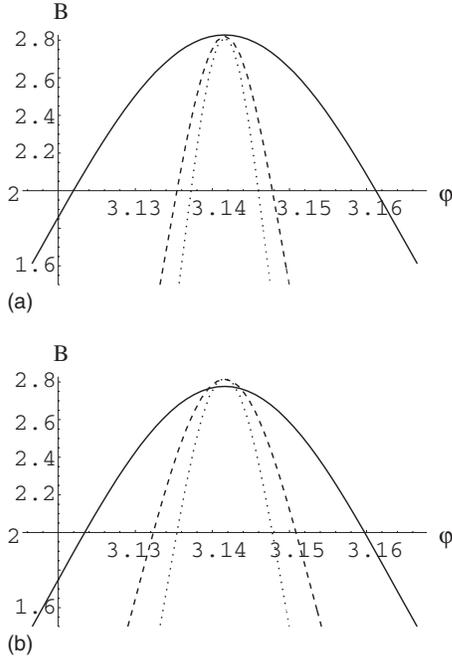
FIG. 7. (a) The Bell-CHSH function B against θ $(=\lambda t)$ for V $=1$ (solid curve), $V=10$ (dashed curve), and $V=20$ (dotted curve) for $d=30$. (b) The Bell-CHSH function for $d=10$ (solid curve), $d=20$ (dashed curve), and $d=30$ (dotted curve) for $V=10$. The Bell violations are more sensitive to the interaction time as either V or d increases.

$$\rho^{\psi} = \int d^2\alpha P_\alpha^{th}(V,d)(a|\alpha\rangle + b|-\alpha\rangle)(a^*\langle\alpha| + b^*\langle-\alpha|),$$

(23)

which can be understood as a generalization of the coherent-state qubit $a|d\rangle + b|-d\rangle$, where $|d\rangle$ is a coherent state of amplitude d. The thermal-state qubit (23) becomes identical to the coherent-state qubit when $V=1$.

We also define four thermal-Bell states as

$$\rho^{\Phi(\pm)} = N_t\{\rho^{th}(V,d) \otimes \rho^{th}(V,d) \pm \sigma(V,d) \otimes \sigma(V,d) \pm \sigma(V,-d)$$
$$\otimes \sigma(V,-d) + \rho^{th}(V,-d) \otimes \rho^{th}(V,-d)\},$$

(24)

$$\rho^{\Psi(\pm)} = N_t\{\rho^{th}(V,d) \otimes \rho^{th}(V,-d) \pm \sigma(V,d) \otimes \sigma(V,-d)$$
$$\pm \sigma(V,-d) \otimes \sigma(V,d) + \rho^{th}(V,-d) \otimes \rho^{th}(V,d)\},$$

(25)

where N_t was defined in Eq. (18). The thermal-Bell states can be written as

$$\rho^{\Phi(\pm)} = N_t \int d\alpha^2 d\beta^2 P_\alpha^{th}(V,d)P_\beta^{th}(V,d)(|\alpha,\beta\rangle \pm |-\alpha,-\beta\rangle)$$
$$\times(\langle\alpha,\beta| \pm \langle-\alpha,-\beta|),$$

(26)

(a)

(b)
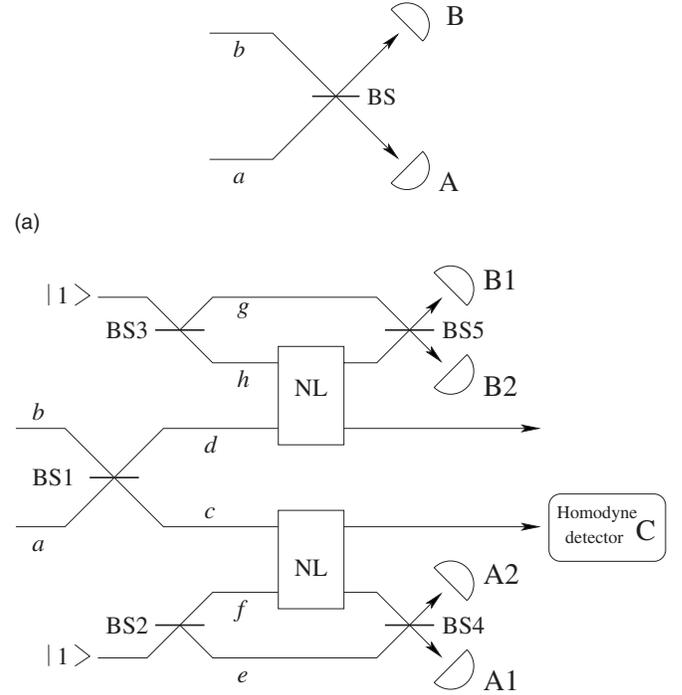
FIG. 8. A schematic of the thermal-Bell state measurement (a) using photon number resolving detection and (b) using homodyne measurements with cross-Kerr nonlinear interactions (NL) (see text for details).

$$\rho^{\Psi(\pm)} = N_t \int d\alpha^2 d\beta^2 P_\alpha^{th}(V,d)P_\beta^{th}(V,d)(|\alpha,-\beta\rangle \pm |-\alpha,\beta\rangle)$$
$$\times(\langle\alpha,-\beta| \pm \langle-\alpha,\beta|).$$

(27)

For quantum-information processing applications, it is an important task to discriminate between the four Bell states. Here we discuss two possible ways to discriminate between the thermal-Bell states (25). We shall only briefly describe the first scheme using photon number resolving measurements and focus on the second scheme using nonlinear interactions.

The first method is to simply use a 50-50 beam splitter and two photon number resolving detectors as shown in Fig. 8(a). This scheme is basically the same as the Bell-state measurement scheme with pure entangled coherent states [25,26]. Let us suppose that the amplitude d is large enough, i.e., $d \gg \sqrt{V}$. If the incident state was $\rho^{\Phi(+)}$ or $\rho^{\Phi(-)}$, most of the photons are detected on detector A in Fig. 8(a). Meanwhile, most of the photons are detected on detector B when the incident state was $\rho^{\Psi(+)}$ or $\rho^{\Psi(-)}$. The average photon numbers between the "many-photon case" and the "few-photon case" are compared in Fig. 9. Furthermore, the states $\rho^{\Psi(+)}$ and $\rho^{\Phi(+)}$ contain only even numbers of photons while $\rho^{\Psi(-)}$ and $\rho^{\Phi(-)}$ contain only odd numbers of photons. Therefore, all the four Bell states can be well discriminated by analyzing numbers of photons detected at detectors A and B. For example, if detector A detects many photons while detector B detects few and the total photon number detected by the two detectors are even, this means that state $\rho^{\Phi(+)}$ was
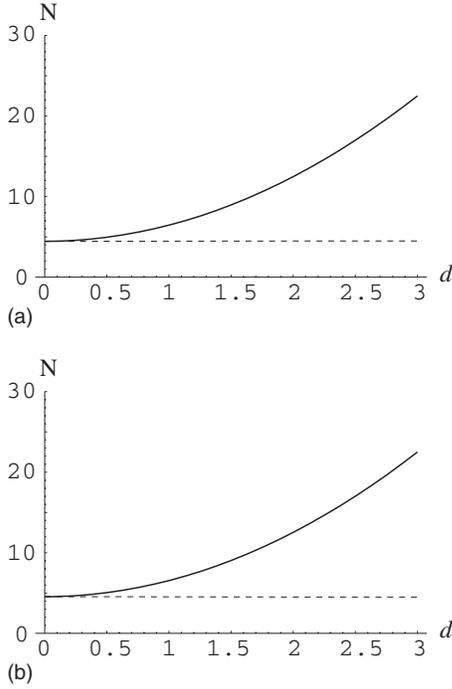
FIG. 9. The average photon number N for the "many-photon case" (solid line) and the "few-photon case" (dashed line) for V $=10$ against d (a) when the input state is either $\rho^{\Phi(+)}$ or $\rho^{\Psi(+)}$ and (b) when the input state is either $\rho^{\Phi(-)}$ or $\rho^{\Psi(-)}$.

measured by the thermal-Bell measurement. The nonzero failure probability can be made arbitrarily small by increasing d.

However, the average photon numbers of the thermal-Bell states are high when $V \gg 1$ and $d \gg 1$. In this case, it would be unrealistic to use photon number resolving detectors. It would be an interesting question whether these four thermal-Bell states can be distinguished by classical measurements, such as homodyne detection, instead of photon number resolving detection. Our alternative scheme employs cross-Kerr nonlinearities and single-photon detectors as shown in Fig. 8(b). Let us first suppose that the input field was $\rho^{\Phi(+)}$. The incident two-mode state passes through a 50-50 beam splitter BS1. The state after passing through the 50:50 beam splitter BS1 is

$$\rho^B = N_t \int d^2\alpha d^2\beta P_\alpha^{\text{th}}(V,d) P_\beta^{\text{th}}(V,d) \{ |\eta, -\xi\rangle\langle\eta, -\xi|$$
$$+ |\eta, -\xi\rangle\langle -\eta, \xi| + |-\eta, \xi\rangle\langle\eta, -\xi| + |-\eta, \xi\rangle\langle -\eta, \xi| \}, \tag{28}$$

where $\eta = (\alpha + \beta)/\sqrt{2}$ and $\xi = (\alpha - \beta)/\sqrt{2}$. Two dual-rail single-photon qubits $|\psi_+\rangle_{ee'}$ and $|\psi_+\rangle_{ff'}$, where

$$|\psi_+\rangle = \frac{1}{\sqrt{2}}(|0\rangle|1\rangle + |1\rangle|0\rangle), \tag{29}$$

are prepared using two single photons and 50:50 beam splitters BS2 and BS3, as shown in Fig. 8(b). Then, traveling fields at modes c and d interact with those of modes e and f,

respectively, in cross-Kerr nonlinear media. We suppose that the interaction time is $t = \pi/\lambda$, and the resulting state is then

$$\rho^{B'} = U_{ce} U_{df} \rho_{cd}^{\mathcal{B}} \rho_{ee'}^q \rho_{ff'}^q U_{ce}^\dagger U_{df}^\dagger, \tag{30}$$

where $U_{ce} = \exp[i\pi \mathcal{H}_{ce}^K/\lambda\hbar]$ and $\rho^q = |\psi_q\rangle\langle\psi_q|$. An explicit form of Eq. (30) can then be simply obtained using the identity

$$U_{ce}|\alpha\rangle_c|0\rangle_e = |\alpha\rangle_c|0\rangle_e,$$

$$U_{ce}|\alpha\rangle_c|1\rangle_e = |-\alpha\rangle_c|1\rangle_e, \tag{31}$$

where $|\alpha\rangle$ is a coherent state. However, we omit such an explicit expression in this paper for it is too lengthy.

After the nonlinear interactions, the qubit parts, modes e, e', f, and f', should be measured with the measurement basis

$$\{|++\rangle, |+-\rangle, |-+\rangle, |--\rangle\}, \tag{32}$$

where $|++\rangle = |\psi_+\rangle_{ee'}|\psi_+\rangle_{ff'}$, $|+-\rangle = |\psi_+\rangle_{ee'}|\psi_-\rangle_{ff'}$, $|-+\rangle = |\psi_-\rangle_{ee'}|\psi_+\rangle_{ff'}$, $|--\rangle = |\psi_-\rangle_{ee'}|\psi_-\rangle_{ff'}$, and $|\psi_-\rangle = (|0\rangle|1\rangle - |1\rangle|0\rangle)/\sqrt{2}$. This measurement can be performed using two 50:50 beam splitters BS4 and BS5, and four detectors $A1$, $A2$, $B1$, and $B2$, as shown in Fig. 8(b). If detectors $A1$ and $B1$ click, i.e., the measurement result is $|++\rangle$, the resulting state at modes c and d is

$$\rho^{++} = \frac{N_t}{4} \int d^2\alpha d^2\beta P_\alpha^{\text{th}}(V,d) P_\beta^{\text{th}}(V,d) \{ (|\eta\rangle + |-\eta\rangle)$$
$$\times (\langle\eta| + \langle -\eta|) \}_c \otimes \{ (|\xi\rangle + |-\xi\rangle)(\langle\xi| + \langle -\xi|) \}_d. \tag{33}$$

Note that state ρ^{++} is not normalized, which implies that the probability of obtaining the corresponding measurement result is not unity. The probability of obtaining this result is

$$P_{++} = \frac{(V+1)(V + e^{-4d^2/V})}{2(V^2 + e^{-4d^2/V})}. \tag{34}$$

When the result is either $|+-\rangle$ or $|-+\rangle$, the result is

$$\langle\psi_2|\rho^{B'}|\psi_2\rangle = \langle\psi_3|\rho^{B'}|\psi_3\rangle = 0, \tag{35}$$

which obviously means that the probability of obtaining this result is zero. When the result is $|--\rangle$, i.e., detectors A2 and B2 click,

$$\rho^{--} = \frac{N_t}{4} \int d^2\alpha d^2\beta P_\alpha^{\text{th}}(V,d) P_\beta^{\text{th}}(V,d)$$
$$\times \{ (|\eta\rangle - |-\eta\rangle)(\langle\eta| - \langle -\eta|) \}_c$$
$$\otimes \{ (|\xi\rangle - |-\xi\rangle)(\langle\xi| - \langle -\xi|) \}_d, \tag{36}$$

which is not normalized. The probability of obtaining this result is

$$P_{--} = \frac{(V-1)(V - e^{-4d^2/V})}{2(V^2 + e^{-4d^2/V})}, \tag{37}$$

and it can be simply verified that $P_{++} + P_{--} = 1$. Therefore, only the measurement results $|++\rangle$ and $|--\rangle$ can be obtained

in the case of the input state $\rho^{\Phi(+)}$. This is exactly the same for the case of $\rho^{\Psi(+)}$. In the same way, it can be shown that if either the input state was $\rho^{\Phi(-)}$ or $\rho^{\Psi(-)}$, only the measurement results $|+-\rangle$ and $|-+\rangle$ can be obtained. In other words, the parity of the total incoming state is perfectly well discriminated by the measurements on single-photon qubits.

Subsequently, a homodyne measurement is performed for mode c by homodyne detector C as shown in Fig. 8(b). We assume that ideal homodyne measurements are performed, i.e., when a homodyne measurement is performed the state is projected onto eigenstate $|x\rangle$ of operator X with eigenvalue x, where

$$X = \frac{1}{\sqrt{2}}(a + a^{\dagger}). \tag{38}$$

Let us first consider the case when the measurement result for the single-photon qubits is $|++\rangle$. In this case, the remaining state is ρ^{++} in Eq. (33). The probability distribution $P^{++}_{\Phi(+)}$ for the homodyne measurement at detector C is

$$P^{++}_{\Phi(+)} = \langle x|\mathrm{Tr}_d[\rho^{++}]|x\rangle = \frac{V^{1/2}(e^{-Vx^2} + e^{-x^2/V})}{\pi^{1/2}(V+1)}. \tag{39}$$

Note that the superscript $++$ denotes that the qubit measurement result was $|++\rangle$, and the subscript $\Phi^{(+)}$ denotes that the input state was $\rho^{\Phi^{(+)}}$. These notations will be used also for the other cases in this section. The same analysis can be performed for the other possible measurement outcome $|--\rangle$ as follows:

$$P^{--}_{\Phi(+)} = \langle x|\mathrm{Tr}_d[\rho^{--}]|x\rangle = \frac{V^{1/2}(e^{-Vx^2} - e^{-x^2/V})}{\pi^{1/2}(V-1)}. \tag{40}$$

In the same way, for another input state $\rho^{\Phi(-)}$ it is straightforward to show

$$P^{+-}_{\Phi(-)} = P^{++}_{\Phi(+)}, \quad P^{-+}_{\Phi(-)} = P^{--}_{\Phi(+)}, \tag{41}$$

and $P^{++}_{\Phi(-)} = P^{--}_{\Phi(-)} = 0$. On the other hand, if the input state was $\rho^{\Psi(+)}$, the probability distributions $P^{++}_{\Psi(+)}$ and $P^{--}_{\Psi(+)}$ at detector C are

$$P^{++}_{\Psi(+)} = \langle x|\mathrm{Tr}_c[\rho^{++}]|x\rangle = \frac{V^{1/2}e^{-[x\{4d+(2+V^2)x\}/V]}\{e^{[(1+V^2)x^2/V]} + 2e^{[2x(2d+x)/V]} + e^{[x(8d+x+V^2x)/V]}\}}{2\pi^{1/2}(e^{4d^2/V}V) + 1}, \tag{42}$$

$$P^{--}_{\Psi(+)} = \langle x|\mathrm{Tr}_c[\rho^{--}]|x\rangle = \frac{V^{1/2}e^{-[x\{4d+(2+V^2)x\}/V]}\{e^{[(1+V^2)x^2/V]} - 2e^{[2x(2d+x)/V]} + e^{[x(8d+x+V^2x)/V]}\}}{2\pi^{1/2}(e^{4d^2/V}V) - 1}. \tag{43}$$

It is straightforward to show for the other input state $\rho^{\Psi(-)}$,

$$P^{+-}_{\Psi(-)} = P^{--}_{\Psi(+)}, \quad P^{-+}_{\Psi(-)} = P^{++}_{\Psi(+)}. \tag{44}$$

The probability distributions $P^{++}_{\Phi(\pm)}$ and $P^{++}_{\Psi(\pm)}$ are plotted in Fig. 10. Figure 10 shows that when the input state was $\rho^{\Phi(+)}$ or $\rho^{\Phi(-)}$, the homodyne measurement outcome by detector C, characterized by $P^{++}_{\Phi(+)}$ and $P^{--}_{\Phi(+)}$, is located around the origin. However, when the input state was $\rho^{\Psi(+)}$ or $\rho^{\Psi(-)}$, the homodyne measurement outcome by detector C, characterized by $P^{++}_{\Psi(+)}$ and $P^{--}_{\Psi(+)}$, is located far from the origin. Therefore, two of the Bell states $\rho^{\Phi(+)}$ or $\rho^{\Phi(-)}$, can be well distinguished from the other two by the homodyne detector C for the case of the measurement outcome $|++\rangle$. Finally, by combining the homodyne measurement result and the qubit measurement result, all four Bell states can be effectively distinguished. For example, let us assume that the measurement outcome of the single photon detectors was $|++\rangle$ and the homodyne detection outcome was around the origin, i.e., $x \approx 0$. Then, one can say that state $\rho^{\Psi(-)}$ has been measured for the result of the thermal-Bell measurement.

As implied in Fig. 10, the overlaps between the probability distributions around the origin, $P^{++}_{\Phi(+)}$ and $P^{--}_{\Phi(+)}$, and the other distributions, $P^{++}_{\Psi(+)}$ and $P^{--}_{\Psi(+)}$, are extremely small for a

sufficiently large d. In other words, the distinguishability by the homodyne detection rapidly approaches 1 as d increases. As an example, we can calculate the distinguishability between the states $\rho^{\Psi(+)}$ and $\rho^{\Phi(+)}$ by the homodyne measurement by detector C. The distinguishability by homodyne detection is

$$\mathcal{P}_s = \frac{1}{2}\left\{\int_{|x|<d} dx P^{++}_c(x) + \int_{|x|\geq d} dx P^{++}_d(x)\right\}, \tag{45}$$

which is plotted in Fig. 11. The distinguishability is $\mathcal{P}_s \approx 0.99$ for $d=5.5$ ($d=7.8$) when $V=10$ ($V=20$), and it becomes as high as $\mathcal{P}_s > 0.999\,99$ for $d=10$ ($d=15$) when $V =10$ ($V=20$). If necessary, another homodyne measurement can be performed for mode d to enhance distinguishability of the Bell measurement. When the probability distribution at detector C is around the origin that of detector D is far from the origin and vice versa.

Note also that the second scheme using homodyne detection is robust to detection inefficiency compared with the first scheme using photon number resolving measurements. In the first scheme, even if a detector misses only one photon, it will result in a completely wrong measurement outcome. In the second scheme, however, the measurement out-
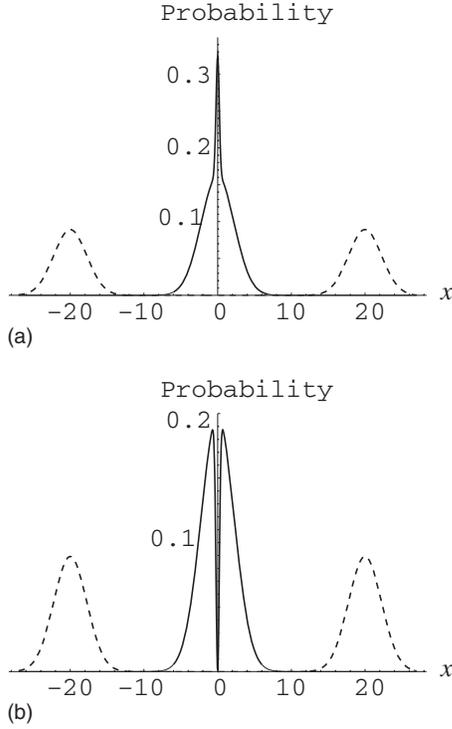
FIG. 10. (a) The probability distributions $P_{\Phi(+)}^{++}$ (solid curve) and $P_{\Psi(+)}^{++}$ (dashed curve) for homodyne measurements at detector C. (b) The probability distributions $P_{\Phi(-)}^{++}$ (solid curve) and $P_{\Psi(-)}^{++}$ (dashed curve) for homodyne measurements at detector C.

come will not be affected in that way. If a single-photon detector misses a photon, it will be immediately recognized. Such a case can simply be discarded so that it will only degrade the success probability of the Bell measurement. The homodyne detection inefficiency will not significantly affect the result when the distributions around the origin and the distributions far from the origin are well separated, i.e., when $d \gg \sqrt{V}$, as shown in Fig. 10. On the other hand, loss in the Kerr medium will have a detrimental affect.

B. Quantum teleportation and computation

Quantum teleportation of a thermal-state qubit can be performed using one of the Bell states as the quantum channel. Let us assume that Alice needs to teleport a thermal-state
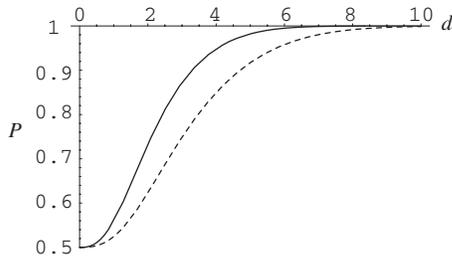
FIG. 11. The distinguishability P_s between states $\rho^{\Psi(+)}$ and $\rho^{\Phi(+)}$ by a homodyne measurement for $V=10$ (solid curve) and $V=20$ (dashed curve) against distance d (see text for details).

qubit ρ^ψ to Bob using a thermal-state entanglement $\rho^{\Psi(-)}$ shared by the two parties. The total state can be represented as

$$\rho_1^\psi \otimes \rho_{23}^{\Psi(-)} = N_t \int d\alpha^2 d\beta^2 d\gamma^2 P_\alpha^{\mathrm{th}}(V,d) P_\beta^{\mathrm{th}}(V,d) P_\gamma^{\mathrm{th}}(V,d)$$
$$\times [(a|\alpha\rangle + b|-\alpha\rangle)_1 (|\beta,-\gamma\rangle - |-\beta,\gamma\rangle)_{23}][\mathrm{H.c.}].$$
(46)

Alice first needs to perform the thermal-Bell measurement described in the previous subsection. To complete the teleportation process, Bob should perform an appropriate unitary transformation on his part of the quantum channel according to the measurement result sent from Alice via a classical channel. It is straightforward to show that the required transformations are exactly the same as those for the coherent-state qubit [25]. When the measurement outcome is $\rho^{\Psi(-)}$, Bob obtains a perfect replica of the original unknown qubit without any operation. When the measurement outcome is $\rho^{\Phi(-)}$, Bob should perform $|\alpha\rangle \leftrightarrow |-\alpha\rangle$ on his qubit in Eq. (23). Such a phase shift by π can be done using a phase shifter whose action is described by $P(\varphi) = e^{i\varphi a^\dagger a}$, where a and $a^\dagger$ are the annihilation and creation operators. When the outcome is $\rho^{\Psi(+)}$, the transformation should be performed as $|\alpha\rangle \rightarrow |\alpha\rangle$ and $|-\alpha\rangle \rightarrow -|-\alpha\rangle$. It is known that the displacement operator is a good approximation of this transformation for $d \gg 1$ [27]. This transformation can also be achieved by teleporting the state again locally and repeating until the required phase shift is obtained [28]. When the outcome is $\rho^{\Phi(+)}$, σ_x and σ_z should be successively applied.

V. CONCLUSION

In this paper, we have studied the characteristics of superpositions and the entanglement of thermal states at high temperatures and discussed their applications to quantum-information processing. The superpositions and entanglement of thermal states show various nonclassical properties such as interference patterns, negativity of the Wigner functions, and violations of the Bell-CHSH inequality. The Bell violations are more sensitive to the interaction time during the generation process when the thermal temperature (i.e., mixedness) of the thermal-state entanglement is larger. Therefore, in order to observe the Bell violations using the mixed state at a high temperature, the interaction time in the Kerr medium should be accurate. We have pointed out that certain superpositions of high-temperature thermal states, symmetric in the phase space, can also be generated. Some of these states have neither squeezing properties nor negative values in their Wigner functions but they are found to be highly nonclassical.

We have introduced the thermal-state qubit and thermal-Bell states for applications to quantum-information processing. We have presented two possible methods for the Bell-state measurement. The Bell-state measurement enables one to perform quantum teleportation and gate operations for quantum computation with thermal-state qubits. The first scheme uses two photon number resolving detectors and a

50-50 beam splitter to discriminate the thermal-Bell states. Using the second scheme, it is possible to effectively discriminate the thermal-Bell states without photon number resolving detection. The required resources for the second scheme are two Kerr nonlinear interactions, two single-photon detectors, two 50:50 beam splitters, and one homodyne detector. The second scheme is more robust to inefficiency of the detectors: the inefficiency of the single-photon detectors only degrades the success probability of the Bell measurement.

[1] E. Schrödinger, Naturwiss. **23**, 807 (1935); **23**, 823 (1935); **23**, 844 (1935).

[2] M. A. Nielsen and I. L. Chuang, *Quantum Computation and Quantum Information* (Cambridge, Cambridge, England, 2000).

[3] H. M. Wiseman and J. A. Vaccaro, Phys. Rev. Lett. **87**, 240402 (2001); see discussions in the Introduction and references therein.

[4] H. Jeong and T. C. Ralph, Phys. Rev. Lett. **97**, 100401 (2006).

[5] E. Schrödinger, Naturwiss. **14**, 664 (1926).

[6] W. Schleich, M. Pernigo, and F. L. Kien, Phys. Rev. A **44**, 2172 (1991).

[7] L. M. Johansen, Phys. Lett. A **329**, 184 (2004).

[8] S. Bose, I. Fuentes-Guridi, P. L. Knight, and V. Vedral, Phys. Rev. Lett. **87**, 050401 (2001).

[9] R. Filip, M. Dusek, J. Fiurasek, and L. Mista, Phys. Rev. A **65**, 043802 (2002).

[10] A. Ferreira, A. Guerreiro, and V. Vedral, Phys. Rev. Lett. **96**, 060407 (2006).

[11] B. S. Cirel'son, Lett. Math. Phys. **4**, 93 (1980).

[12] V. Vedral, New J. Phys. **6**, 102 (2004).

[13] D. F. Walls and G. J. Milburn, *Quantum Optics* (Springer-Verlag, Berlin, 1994).

[14] M. Brune, E. Hagley, J. Dreyer, X. Maitre, A. Maali, C. Wunderlich, J. M. Raimond, and S. Haroche, Phys. Rev. Lett. **77**, 4887 (1996); A. Auffeves, P. Maioli, T. Meunier, S. Gleyzes, G. Nogues, M. Brune, J. M. Raimond, and S. Haroche, *ibid.* **91**, 230405 (2003).

[15] H. Schmidt and A. Imamoglu, Opt. Lett. **21**, 1936 (1996); L. V. Hau *et al.*, Nature (London) **397**, 594 (1999).

[16] H. Jeong, Phys. Rev. A **72**, 034305 (2005), and references therein.

[17] We note that denominator V was missing in the generation probability $\mathcal{P}_{\pm}$ in [4].

[18] M. S. Kim and J. Lee, Phys. Rev. A **61**, 042102 (2000).

[19] D. M. Greenberger, M. Horne, and A. Zeilinger, *Bellis Theorem, Quantum Theory, and Conceptions of the Universe*, edited by M. Kafatos (Kluwer, Dordrecht, 1989), p. 69.

[20] S. Bell, Physics (Long Island City, N.Y.) **1**, 195 (1964).

[21] J. F. Clauser, M. A. Horne, A. Shimony, and R. A. Holt, Phys. Rev. Lett. **23**, 880 (1969).

[22] K. Banaszek and K. Wódkiewicz, Phys. Rev. A **58**, 4345 (1998); Phys. Rev. Lett. **82**, 2009 (1999).

[23] B.-G. Englert, N. Sterpi, and H. Walther, Opt. Commun. **100**, 526 (1993).

[24] H. Jeong, W. Son, M. S. Kim, D. Ahn, and C. Brukner, Phys. Rev. A **67**, 012106 (2003).

[25] H. Jeong, M. S. Kim, and J. Lee, Phys. Rev. A **64**, 052308 (2001).

[26] S. J. van Enk and O. Hirota, Phys. Rev. A **64**, 022313 (2001).

[27] H. Jeong and M. S. Kim, Phys. Rev. A **65**, 042305 (2002).

[28] T. C. Ralph, A. Gilchrist, G. J. Milburn, W. J. Munro, and S. Glancy, Phys. Rev. A **68**, 042319 (2003).